[American Journal of Science, Vol. 313, February, 2013, P. 61–80, DOI 10.2475/02.2013.01]

American Journal of Science

FEBRUARY 2013

THE IMPACT OF TOPOGRAPHY ON ISOTOPES IN PRECIPITATION ACROSS THE CENTRAL ANATOLIAN PLATEAU (TURKEY)

FABIAN SCHEMMEL*,***, TAMÁS MIKES*,**, BORA ROJAY§, and ANDREAS MULCH*,**,***

ABSTRACT. Paleoelevation reconstructions of mountain belts and orogenic plateaus based on stable isotope climate and precipitation records benefit greatly from present-day calibrations that relate the fractionation of hydrogen (δD) and oxygen ($\delta^{18}O$) isotopes in precipitation to orographic rainfall. Here, we establish a first-order template of δD and $\delta^{18}O$ of modern meteoric waters across the Central Anatolian Plateau (CAP) and its bordering Pontic and Taurus Mountains. We identify key regions in the plateau interior and along the plateau margins that have the potential to reliably record topography-related paleotemperature and paleoprecipitation changes as recovered from stable isotope paleosol, fossil teeth or lipid proxy data. Based on δD and $\delta^{18}O$ data of more than 480 surface water samples from small catchments and springs, we characterize moisture sources affecting the net isotopic budget of precipitation over the CAP and analyze how orographic rainout and plateau aridity shape modern patterns of δD and $\delta^{18}O$ in precipitation. The Taurus Mountains bordering the CAP to the south act as a major orographic barrier for transport of predominantly winter moisture and exhibit isotopic lapse rates of approximately −20‰/km for δD and −2.9‰/km for $\delta^{18}O$ across an elevation range of nearly 3000 m. The Pontic Mountains at the northern margin of the CAP force perennial moisture to ascend and condensate revealing lapse rates of −19‰/km for δD and −2.6‰/km for $\delta^{18}O$. The difference in the predominant moisture source for the southern and northern margins of the CAP (North African versus Atlantic air masses) is manifested in systematic north-south differences in near-sea level meteoric water compositions of $\Delta(\delta D_{N\text{-}S})$ ~20 permil and $\Delta(\delta^{18}O_{N\text{-}S})$ ~3 permil in a swath across the central part of the plateau. Stable isotope data from the semi-arid plateau interior with rainfall as low as 300 to 500 mm/yr and mean summer temperatures attaining 23 °C, provide clear evidence for an evaporative regime that drastically affects surface water and runoff compositions and results in a local meteoric water line for the plateau interior that follows $\delta D = 4.0 \cdot \delta^{18}O - 29.3$. Strongly evaporitic conditions contrast rainfall patterns along the plateau margins including their immediate leeward flanks where δD- and $\delta^{18}O$-elevation relationships are reliable predictors of modern topography.

Key words: Central Anatolian Plateau, meteoric water, precipitation, hydrogen isotopes, oxygen isotopes, paleoaltimetry

* Biodiversity and Climate Research Centre (BiK-F), Senckenberganlage 25, D-60325 Frankfurt am Main, Germany; fabian.schemmel@senckenberg.de, andreas.mulch@senckenberg.de

** Goethe University, Institute of Geosciences, Altenhöferallee 1, D-60438 Frankfurt am Main, Germany; mikes@em.uni-frankfurt.de

*** Senckenberg Research Institute and Natural History Museum, Senckenberganlage 25, D-60325 Frankfurt am Main, Germany

§ Middle East Technical University, Institute of Geological Engineering, TR-06531, Ankara, Turkey; brojay@metu.edu.tr

INTRODUCTION

Why Stable Isotope Paleoaltimetry in Anatolia?

Reconstructing paleoelevation of major mountain belts and continental plateau regions such as Tibet, the Andes, or western North America plays an important role in relating Earth surface dynamics to the geodynamic processes of the Earth's interior. Stable isotope paleoaltimetry, despite being a relatively young field, has been instrumental in many of such studies (for example, Chamberlain and others, 1999; Garzione and others, 2000a, 2000b; Rowley and others, 2001; Horton and others, 2004; Currie and others, 2005; Cyr and others, 2005; Garzione and others, 2006; Mulch and others, 2006; Rowley and Currie, 2006; Mulch and Chamberlain, 2007; Mulch and others, 2008; Garzione and others, 2008; Mulch and others, 2010; Quade and others, 2011; Mix and others, 2011; Campani and others, 2012). Stable isotope paleoaltimetry builds on the orographic rainout effect, the thermodynamically controlled systematic decrease of stable hydrogen (δD) and oxygen (δ^{18}O) isotope ratios in precipitation with increasing elevation and hence decreasing condensation temperatures on the windward side of a mountain range. This process is commonly accompanied by the development of an "isotopic rain shadow," a zone of local stable isotopic minima confined to the immediate leeward side, where the isotopic values are mostly controlled by the elevation of the range alone (for example, Dansgaard, 1964; Ingraham and Taylor, 1991; Blisniuk and Stern, 2005). Recovery of the spatio-temporal changes in the hydrogen and oxygen isotopic composition of authigenic minerals may hence reveal changes in paleoclimate and track the evolution of regional topography (for example, Quade and others, 2007; Mulch and Chamberlain, 2007). However, uncertainties in reconstructing past rainfall-topography relationships can arise with the interplay of certain climatic and/or topographic conditions such as (1) upstream changes in the source area of water vapor, (2) variable air parcel trajectories, (3) mixing of air masses or evaporation of meteoric waters under (semi-)arid climate regimes, or (4) changes in stable isotope in precipitation-elevation relationships ("isotopic lapse rate") over geologic time. These factors can mask δD and δ^{18}O signals in the geologic record and may lead to over- or underestimation of past changes in climate and topography (for example, Ehlers and Poulsen, 2009; Galewsky, 2009; Insel and others, 2009; Poulsen and others, 2010; Vachon and others, 2010; Lechler and Niemi, 2011).

Despite its important role in the Mediterranean geodynamic and climate history, little is known about the Neogene elevation history of the Central Anatolian Plateau (CAP). Being the third largest orogenic plateau on Earth, it is situated in the Alpine-Himalayan orogenic belt in the Eastern Mediterranean. The CAP shares many of the characteristics of the large continental plateau regions: aridity and relatively subdued topography in the plateau interior as well as high-elevation plateau-bounding mountain ranges, albeit on an overall smaller scale than, for example, the Altiplano and Tibet (fig. 1A). Located in a progressively changing stress field between the collision zone of Africa and Arabia with Eurasia in the E and the back-arc extensional province behind the Aegean subduction zone in the W, principal driving mechanisms of elevation gain in the CAP region involve both (1) mantle upwelling due to slab tear of the northward-dipping, downgoing African plate (at the southern plateau margin; Gans and others, 2009; Biryol and others, 2011; Cosentino and others, 2012; Schildgen and others, 2012a, 2012b) and (2) upper crustal shortening (at the northern plateau margin; Yildirim and others, 2011). The onset of accelerated surface uplift of the plateau margins dates back to about 8 to 7 Ma in the south (Cosentino and others, 2012; Schildgen and others, 2012b) and to the Late Miocene to Early Pliocene in the north (Yildirim and others, 2011). As suggested by numerical paleotopographic reconstructions and by apatite fission track thermochronology respectively, both

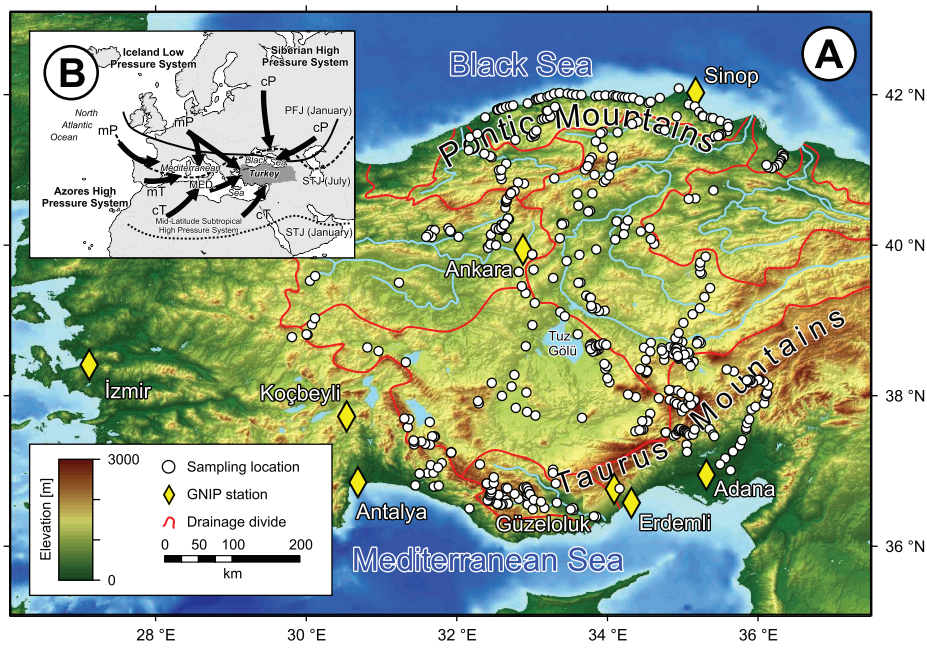

Fig. 1. (A) Digital elevation model of the Central Anatolian Plateau showing sample locations as well as selected meteorological stations of the Global Network of Isotopes in Precipitation (GNIP; IAEA/WMO, 2006; see text for details). (B) Schematic diagram of major air masses affecting Anatolian climate (modified after Sariş and others, 2010). Abbreviations: cP, continental polar air mass; cT, continental tropical air mass; MED, Mediterranean air mass; mP, marine polar air mass; mT, marine tropical air mass; PFJ, Polar Front Jet; STJ, Sub-tropical Jet.

margins were to some extent characterized by topographic relief before the onset of the major uplift (Cavazza and others, 2011; Schildgen and others, 2012b). The youngest marine sediments in the CAP interior are Eocene in age (Lüttig and Steffens, 1975; Görür and Tüysüz, 2001).

The CAP therefore lends itself favorably for reconstructing the coupled geodynamic, climatic, and Earth surface processes that together shaped its modern topography. The topographic history of Central Anatolia over the past 10 Ma plays a key role in understanding the interplay between lithospheric-scale geodynamic processes and Earth surface dynamics, due to the tight links between the Late Neogene-to-recent dynamics of the Mediterranean slab subducting beneath Anatolia, slab break-off, asthenospheric upwelling, continental volcanism, seismicity, brittle tectonics, and surface uplift (Şengör and others, 2005; Biryol and others, 2011; Cosentino and others, 2012; Schildgen and others, 2012a, 2012b). Equally important is the role of Central Anatolian Earth surface dynamics in controlling regional climate patterns and the development of ecosystems in the Eastern Mediterranean; one of the crossroads of hominids between Africa and Eurasia (Görür and others, 1995; Müller and others, 2011).

Topographic and Climatic Setting

Bordered by two E-W trending mountain ranges roughly 400 km apart, the CAP attains an average elevation of about 1000 m. To the N along the Black Sea coast, the Pontic Mountains reach average elevations of up to 1400 m, while the Taurus Mountains along the Mediterranean coast to the S are characterized by an average

elevation of about 2400 m with highest peaks attaining 3756 m (Demirkazık Dağı) (fig. 1A). Atmospheric moisture is transported to Anatolia by two principal air masses that are sourced in the polar and in the tropical regions (fig. 1B). Winter precipitation is connected primarily to the Icelandic Low Pressure System above the N Atlantic and the Mediterranean Depression as well as to anticyclones controlled by the Azores High Pressure System and subordinately to the stable, continental high-pressure systems centered above Siberia. Summer rains are brought by continental tropical air masses sourced in Northern Africa that typically merge en route with Arabian and Middle Eastern systems before reaching the Anatolian region (Türkeş and Erlat, 2005). The modern climate of Anatolia is diverse, with topography exerting a strong control on precipitation and temperature distribution (fig. 2). It is temperate, semi-humid to humid in the coastal regions where the bulk of annual precipitation occurs (Türkeş and Erlat, 2005). The plateau interior in contrast is semi-arid and characterized by hot and dry summers and cold winters. Mean annual temperatures (MAT) in the northern part of the CAP of about 9 °C are slightly lower than in the south (12 °C). The mean temperature of the driest (summer) months is approximately 23 °C (−2 °C in the winter months). Mean annual temperatures of up to 20 °C characterize the Mediterranean coast whereas the Black Sea coast is uniformly colder (MAT of about 13 °C). Mean summer (winter) temperatures in the coastal regions close to sea level are 23 °C (7 °C) in the N and 29 °C (9 °C) in the S (Sensoy and others, 2008). Most of the precipitation on the plateau falls between December and May, amounting to 300 to 500 mm/yr, with a slight S-to-N increase. Summer precipitation however is very limited and usually does not balance the water deficit that emerges during the warm, dry, evaporation-dominated summer months (Sensoy and others, 2008; Ankara in fig. 2C). The coastal mountain fronts receive more than 1000 mm/yr orographic precipitation (Türkeş and Erlat, 2005), largely restricted to the period from October to May with the Pontic Mountains usually being humid over the course of the year.

Goal of This Study

Here we present stable hydrogen (δD) and oxygen ($\delta^{18}O$) isotopic data of modern meteoric waters from the Central Anatolian Plateau in Turkey. We aim (1) to characterize the isotopic composition of moisture transported to Anatolia, and (2) to assess the effects of orographic rainout, the change in isotopic composition of precipitation as a function of elevation ("isotopic lapse rate") on the windward sides of both the Taurus and the Pontic Mountains. We (3) characterize the oxygen and hydrogen isotopic rain shadows on the leeward sides of the Pontic and Taurus mountain ranges, and (4) identify the effects of evaporation on meteoric water δD and $\delta^{18}O$ values within the plateau interior. Based on data from more than 480 stream, creek, and near-surface groundwater samples, we establish a robust first-order isotopic template at the scale of the entire CAP and its margins, against which continental paleoclimate proxy data can be interpreted.

Sampling Strategy

For surface water sampling, we focused on streams and creeks from small catchments as well as tapped springs (locally referred to as çeşme). This approach, besides a large spatial coverage, has distinct advantages over sampling precipitation directly as it provides robust, long-term, yet spatially highly resolved patterns of the isotopic composition of precipitation and near-surface groundwaters by reducing bias (1) from shorter-term, daily to seasonal hydrometeorological variations and (2) from downstream mixing of waters from catchments in markedly different isotopic (climatic and topographic) regimes (Kendall and Coplen, 2001). We tested the robustness of our approach by comparing our data to the precipitation-weighted longer-term (>1

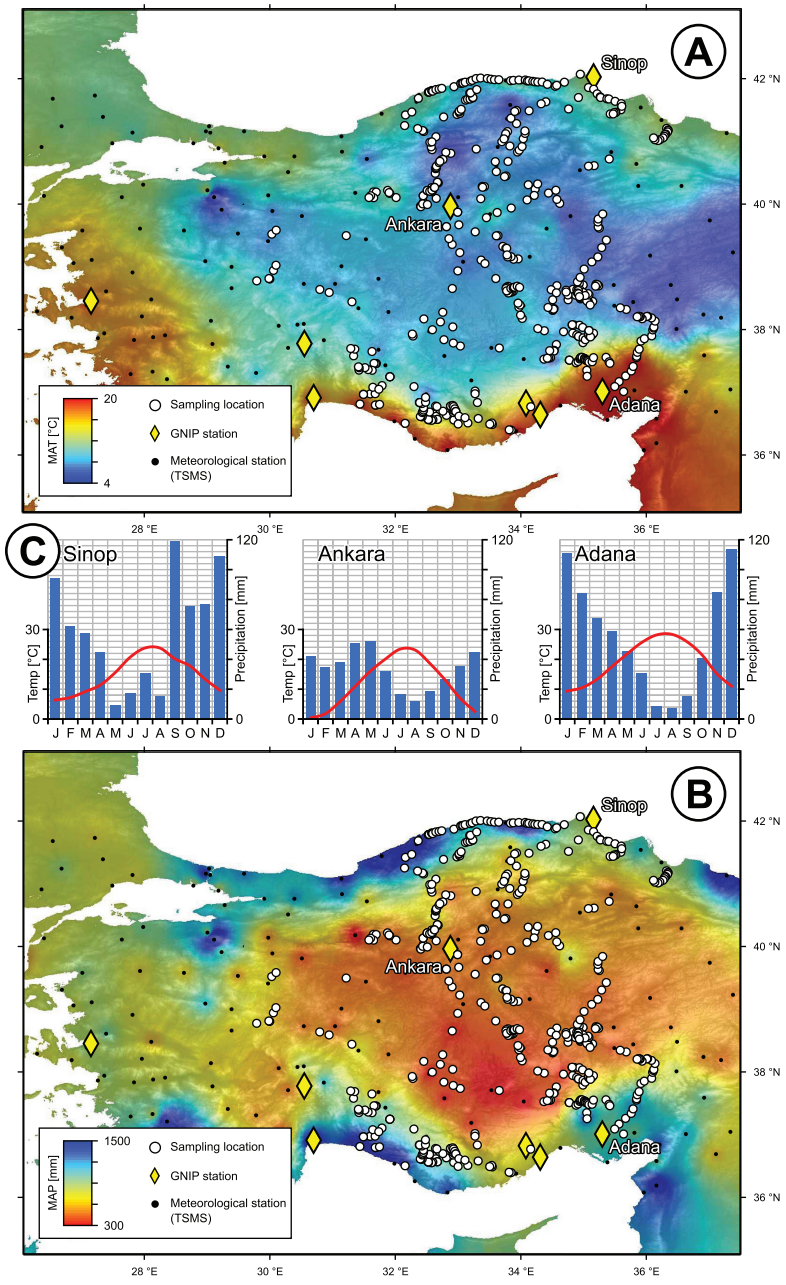

Fig. 2. Distribution of (A) mean annual temperature and (B) mean annual precipitation in Central Anatolia. The maps were calculated by inverse distance-weighted interpolation of long-term data recorded by the station network of the Turkish State Meteorological Survey, Ankara (TSMS; data courtesy of M. Demircan). (C) Long-term mean monthly temperature and precipitation trends of the GNIP stations at Sinop, Ankara, and Adana (IAEA/WMO, 2006).

yr) averages of the monthly δD_p and $\delta^{18}O_p$ data series recorded at the stations of the Global Network of Isotopes in Precipitation (GNIP) in Turkey (IAEA/WMO, 2006; T. Chavez and S. Terzer, personal communication; fig. 1; table 1).

Table 1

Yearly precipitation-weighted mean δD_p and $\delta^{18}O_p$ values of GNIP stations in Central Anatolia (IAEA/WMO, 2006)

GNIP station	WMO code	Elevation (m)	δD_p[SMOW]		$\delta^{18}O_p$[SMOW]		*d* [‰]	instrumental records
			‰	n	‰	n		
Ankara	1713000	902	–52.3	415	–7.93	440	11.2	1963–2009
Antalya	1730000	49	–24.2	299	–4.57	311	12.3	1970–2009
Adana	1735000	73	–22.4	281	–4.34	281	12.3	1978–2009
Erdemli	1735201	10	–35.4	17	–5.56	11	9.1	1991–1993
Güzeloluk	1735202	1400	–48.4	21	–7.67	33	13.0	1990–1993
İzmir	1722000	120	–30.3	14	–5.25	14	11.6	2008–2009
Koçbeyli	1702600	1025	–58.4	35	–8.74	35	11.5	1989–1993
Sinop	1702600	32	–47.0	18	–7.36	16	11.8	2008–2009

Methods

We sampled a total of 482 natural waters from a wide range of elevations that cover most of the area of the Central Anatolian Plateau as well as the Taurus and Pontic Mountains (fig. 1). Several transects were collected from the coasts to the plateau interior to assess the hydrogen and oxygen isotope fractionation that accompanies orographic rainout. Field campaigns took place during the months of May to October from 2008 to 2011 in order to collect the samples under conditions as close to base flow as possible. The sampling elevations cover a range from 0 to 1911 m, with high-elevation locations well represented in both mountain ranges. The sample set consists of 180 surface water samples from streams and creeks as well as 302 spring water samples. At each sampling site 30 ml of unfiltered water were collected in high-density polyethylene bottles, with as little air volume as possible in the closed bottles. Samples were kept at room temperature and in the dark until return to the laboratory for refrigeration and analysis.

Stable hydrogen and oxygen isotope ratio measurements were made on 1 ml aliquots using an LGR 24d liquid isotope water analyzer at the Institute of Geology (University of Hannover) and at the Institute of Geoscience (Goethe University Frankfurt), using identical data acquisition protocols. δD and $\delta^{18}O$ values were corrected based on internal lab standards that are calibrated against SMOW. The analytical precision is typically better than 0.6 permil and 0.2 permil (both 2σ) absolute for δD and $\delta^{18}O$, respectively. Absolute stable isotope values of the sample set range from -24 to $-96‰$ for δD and -4.5 to $-13.0‰$ for $\delta^{18}O$. The entire dataset is provided in table A1 of the electronic supplementary material (http://earth.geology.yale.edu/~ajs/SupplementaryData/2013/01Schemmel.pdf).

Sampling perennial streams, creeks, and springs provides an amount-weighted, long-term average of precipitation characteristic for individual catchments. Determining the elevation at which these catchments are recharged by rainfall is, however, not straightforward (Rowley and others, 2001; Currie and others, 2005; Galewsky, 2009; Quade and others, 2011). Whereas sampling elevations may correlate well with the actual condensation height in small high-elevation catchments significant local relief can lead to an underestimation of the elevation at which the bulk of precipitation occurred and hence obscure isotope–elevation relationships. Therefore, we adopted

an approach of deriving catchment sizes and average catchment elevations (ACEs) for each water sample. Since the relief distribution in the catchment is accounted for by these calculated ACEs, they provide a very good estimate for the catchment-wide hypsometric mean precipitation elevation. We did not attempt to derive precipitation-weighted hypsometric mean elevations due to the lack of high-resolution rainfall data for individual mountain catchments. The ACEs of each sampled water flow were calculated using an elevation-weighted flow accumulation model in ESRI® ArcGIS™ 10.0, based on version 1 of the ASTER Global Digital Elevation Model which has a spatial resolution of 1 arc second (approximately 30 m) and is provided by the Earth Remote Sensing Data Analysis Center, Japan.

RESULTS AND DISCUSSION

Four main features characterize our δD and $\delta^{18}O$ data (fig. 3): (1) Samples along the coasts generally show the least negative δD and $\delta^{18}O$ values with those from the Mediterranean Sea coast being notably higher (about 21‰ in δD and about 3.1 permil in $\delta^{18}O$) compared to samples from the Black Sea coast. (2) Hydrogen and oxygen isotope ratios change systematically across the Pontic and Taurus Mountains and attain the lowest δD and $\delta^{18}O$ values on the leeward sides of both mountain ranges. (3) From the leeward plateau margin towards the plateau center δD and $\delta^{18}O$ both show a trend of increasing δD (about 20 to 25‰) and $\delta^{18}O$ (about 5 to 6‰) values paralleled by a general increase in variability. (4) Deuterium excess (d) is generally high in the coastal areas and decreases towards the plateau interior.

The median catchment size upstream of our 180 surface water samples is 69 km^2, with only a few major rivers draining into the Mediterranean or the Black Sea having catchments up to about 20,000 km^2 upstream the sampling site (table A2 of the electronic supplementary material, http://earth.geology.yale.edu/~ajs/SupplementaryData/2013/01Schemmel.pdf). In any of the identified geographic zones as described below, neither the stable isotope ratios nor the deuterium excess values d show any clear dependence on the sizes of the individual catchments.

Long-Term Stability of δD and $\delta^{18}O$ Values

Our δD and $\delta^{18}O$ values of local streams, creeks, and springs show good agreement with the small number of long-term instrumental records of GNIP stations within the CAP and at its margins (fig. 3). Matching long-term and surface runoff/spring data demonstrates that most of the surface water flows sampled in this study represent modern, longer-term (multi-year to decadal) average rainfall conditions across Central Anatolia. Second, for most of the sampling sites we do not observe a significant difference in the spatial distribution of δD or $\delta^{18}O$ values between stream/creek waters and spring waters (figs. 3C and 3D). The latter observation suggests that at these scales (both temporally and spatially) the majority of the sampled water is representative of local meteoric water. Hence, the sampled springs most likely tap near-surface groundwaters with negligible contribution from deeper, distally derived groundwaters (for a discussion of the effects of distal groundwater sources and residence times see below).

Spatial Distribution of δD and $\delta^{18}O$ Values

We observe a strong difference in near-sea level δD and $\delta^{18}O$ values between the northern and southern coastal regions of the plateau of ≥21 permil for $\Delta(\delta D)_{Taur\text{-}Pont}$ and ≥3.1 permil for $\Delta(\delta^{18}O)_{Taur\text{-}Pont}$ (figs. 3C and 3D). This difference is also visible in different deuterium excess values, defined as $d = \delta D - 8 \cdot \delta^{18}O$ (Craig and Gordon, 1965). d is somewhat higher on the windward flanks of the Taurus Mountains but accompanied by a larger scatter ($d = 18.1 \pm 5.0$) than observed on the northern flanks of the Pontic Mountains ($d = 15.8 \pm 1.9$) (fig. 4). The difference in the initial δD and $\delta^{18}O$ values, (and possibly in d) most likely results from

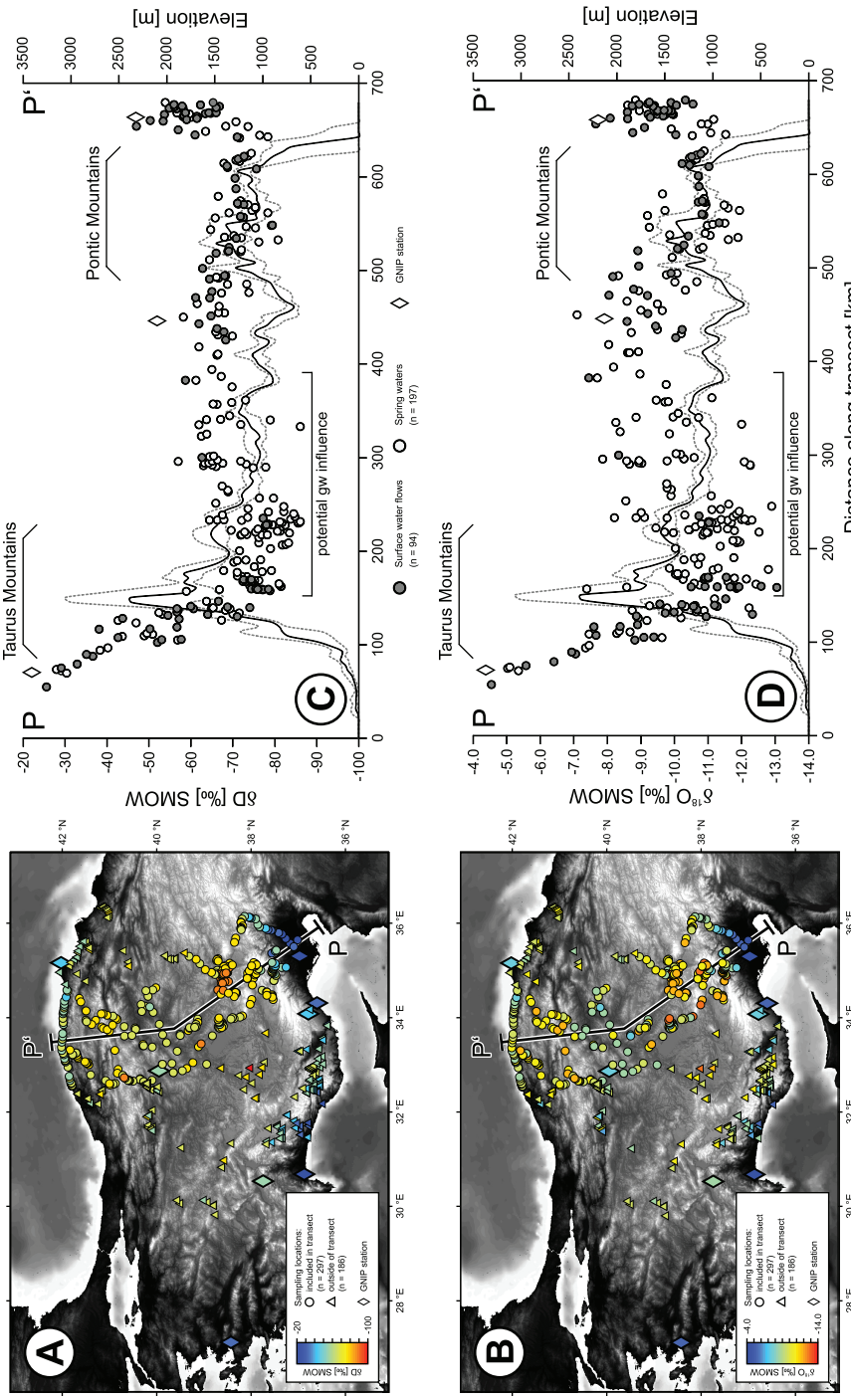

Fig. 3. Spatial distribution of (A) δD and (B) $\delta^{18}O$ over the Central Anatolian Plateau. Sampling transects (C) and (D) pass through the Taurus Mountains, the plateau interior, and the Pontic Mountains and include samples within a 70-km-wide swath along the profile along with the long-term δD_P and $\delta^{18}O_P$ values of the GNIP stations at Adana, Ankara and Sinop (IAEA/WMO, 2006). Elevations (dotted and solid lines) correspond to the Q_{25}, Q_{50} and Q_{75} quantiles of the elevation distribution at any point along the swath profile. The GNIP data from the northernmost station at Sinop are plotted in figures 3C and 3D to facilitate comparison. Area of potential groundwater influence constrained by extent of Konya Closed Basin (fig. 4). See text for details of potential distal groundwater influence.

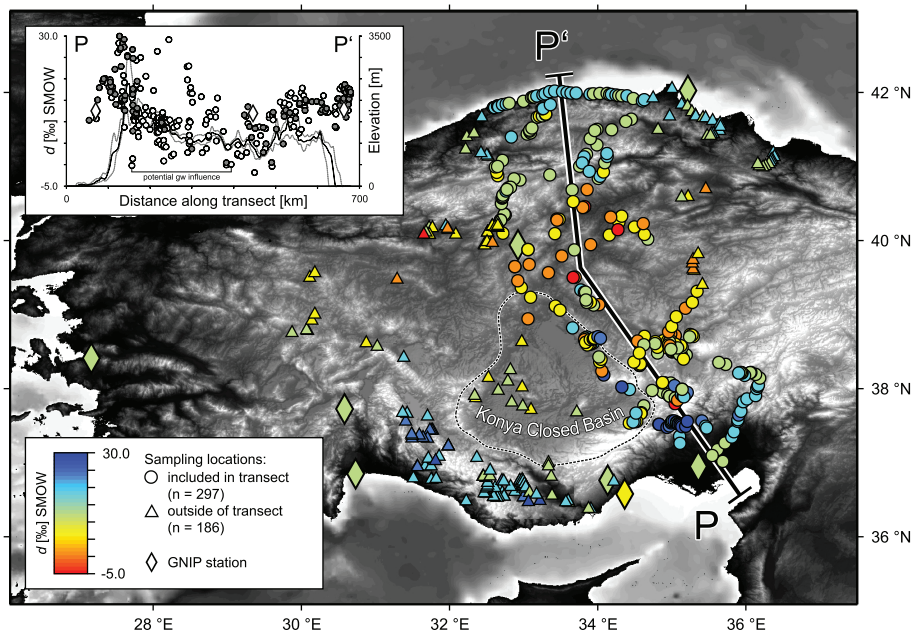

Fig. 4. Spatial distribution of deuterium excess (d) values over the Central Anatolian Plateau. The transect shows d of the samples along with the long-term d of the GNIP stations at Adana, Ankara, and Sinop (IAEA/WMO, 2006). Samples included in the calculation are within a 70-km-wide swath along the profile and elevations (solid and dotted lines in the inset) correspond to the $Q_{.25}$, $Q_{.50}$ and $Q_{.75}$ quartiles of the elevation distribution at any point along the swath profile. Location of the Konya Closed Basin is taken from Bayari and others (2009). See text for details of groundwater influence.

different air parcel trajectories of advected moisture that eventually controls precipitation patterns of Central Anatolia. Overall, the δD and $\delta^{18}O$ data are in excellent agreement with available air mass trajectories that indicate multiple moisture sources (fig. 1B; Rindsberger and others, 1983; Gat and others, 2003; Türkeş, 2003; Dirican and others, 2005; Türkeş and Erlat, 2005; Pfahl and Wernli, 2008; Sariş and others, 2010).

With respect to potential stable isotope paleoaltimetry reconstructions, the strong decrease in both δD and $\delta^{18}O$ values across the Taurus Mountains is one of the most important characteristics of the data presented here (fig. 3). Orographic rainfall produces a decrease in D and ^{18}O that equals about 50 to 60 permil for $\Delta(\delta D)_{\text{windward–leeward}}$ and about 7 to 8 permil for $\Delta(\delta^{18}O)_{\text{windward-leeward}}$ in the Taurus Mountains. We observe a similar decrease yet of smaller magnitude in the Pontic Mountains with $\Delta(\delta D)_{\text{windward–leeward}}$ of about 25 permil and $\Delta(\delta^{18}O)_{\text{windward–leeward}}$ of about 3 permil. Systematic altitude effects on δD and $\delta^{18}O$ in precipitation are characteristic for many of the world's major mountain belts (for example, Dansgaard, 1964; Poage and Chamberlain, 2001; Rowley and Garzione, 2007; Quade and others, 2011). The resulting spatial pattern of low δD and $\delta^{18}O$ values in near-surface groundwater and runoff ("isotopic rain shadow") on the leeward sides of both mountain ranges does not necessarily correlate with regional changes in rainfall amount (figs. 2 and 3). From the immediate lee towards the plateau interior, both δD and $\delta^{18}O$ values show a general increase of about 20 to 25 permil and 5 to 6 permil, respectively. This increase is accompanied by an increasing variability of δD and $\delta^{18}O$ values (fig. 3). We attribute this to the increased aridity within the plateau interior (fig.

2; Sensoy and others, 2008), which promotes secondary (sub-cloud and surface) evaporation of meteoric waters. This conclusion is further supported by the strongly contrasting meteoric water lines of the coastal and plateau regions (see discussion below). Additionally, the increase in δD and $\delta^{18}O$ towards the plateau center could also result from progressive mixing between southerly- and northerly-derived air masses (in the lee of the Taurus and Pontic Mountains, respectively). However, a linear mixing model between the two initial moisture compositions (that is, the most negative δD and $\delta^{18}O$ values) at the leeward flanks in the N and the S (figs. 3C and 3D) alone does not explain the observed high δD and $\delta^{18}O$ values in the plateau interior due to the downward-convex shape of the distribution of isotopic values along the N-S transect. To some extent, admixing of westerly-derived moisture—which has not undergone significant orographic rainout—to the plateau interior is likely, based on the decrease in GNIP-derived δD_p and $\delta^{18}O_p$ values between the Aegean Sea coast (İzmir GNIP station) and the plateau interior (Ankara GNIP station) of −22 permil and −2.7 permil, respectively (table 1; see also figure A1 in the electronic supplementary material; http://earth.geology.yale.edu/~ajs/SupplementaryData/2013/01Schemmel.pdf). Again, whereas this process may not be insignificant, it cannot be entirely accounted for the magnitude of positive isotopic shift towards the plateau interior due to the clear-cut difference in the Meteoric Water Lines between the mountain ranges and the plateau interior, as will be demonstrated in the following section.

Meteoric Water Lines

Most of the surface water samples plot above the Global Meteoric Water Line (GMWL; Craig, 1961) (fig. 5) that follows the general expression $\delta D = 8.17 \cdot \delta^{18}O + 10.35$ (Rozanski and others, 1993). A classification of water samples based on similar stable isotopic trends as well as geographical location shows that samples collected at the windward side of the Taurus and Pontic Mountains, where δD and $\delta^{18}O$ patterns result mostly from the altitude effect (fig. 3), plot in an array parallel to the GMWL and follow the equations:

$$\text{Windward Pontic Mountains LMWL: } \delta D = 7.1 \cdot \delta^{18}O + 7.3 \quad (1)$$

$$\text{Windward Taurus Mountains LMWL: } \delta D = 7.2 \cdot \delta^{18}O + 10.8. \quad (2)$$

In contrast, samples from the plateau interior define a markedly different local meteoric water line (LMWL):

$$\text{Plateau Interior LMWL: } \delta D = 4.0 \cdot \delta^{18}O - 29.3. \quad (3)$$

The good agreement of the LMWLs of both windward mountain flanks (eqs 1 and 2) and the GMWL supports the assumption that surface water flows from the coastal areas consist mainly of runoff from local precipitation that has experienced little to no secondary evaporation. The relatively low slope of 4.0 of the Plateau Interior LMWL (eq 3) indicates that surface water flows on the plateau experienced strong secondary evaporation.

For precipitation originating in the eastern Mediterranean, values of *d* have been reported as high as +20 permil and above (Gat and Carmi, 1970). This translates to an Eastern Mediterranean Water Line (EMWL) of about $\delta D = 8 \cdot \delta^{18}O + 20$. Analysis of available isotopic data of monthly precipitation (δD_p and $\delta^{18}O_p$) obtained through the Turkey GNIP stations in a period from 2001 to 2003 results in a specific Turkish Meteoric Water Line (TMWL) that follows the equation: $\delta D = 7.7 \cdot \delta^{18}O + 13.1$ (Dirican and others, 2005). The TMWL is in good agreement with the LMWLs of both windward mountain flanks presented here (eqs 1 and 2).

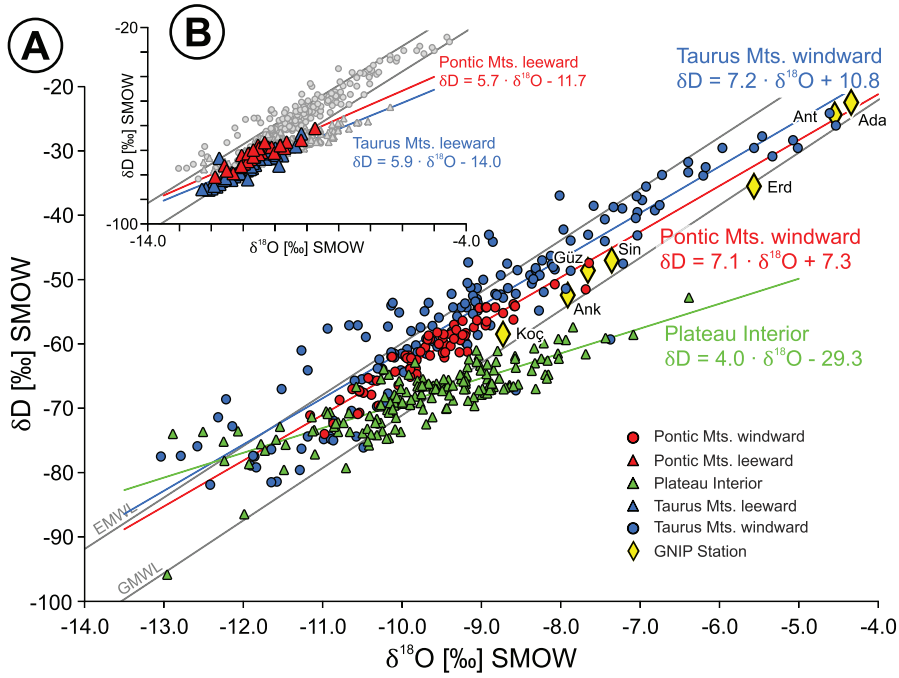

Fig. 5. (A) δD versus $\delta^{18}O$ of water samples collected on the plateau margins (n_{north} = 73, n_{south} = 154) and the plateau interior (n = 172). The corresponding LMWLs are compared to the long-term values of selected GNIP stations (IAEA/WMO, 2006) as well as to the Global Meteoric Water Line (Rozanski and others, 1993) and the Eastern Mediterranean Water Line (Gat and Carmi, 1970). (B) δD versus $\delta^{18}O$ of water samples collected in the rain shadow areas (n_{north} = 36, n_{south} = 47) with corresponding LMWLs. The remaining part of the dataset—as shown in figure 4A—is indicated by gray symbols for comparison. Abbreviations of the GNIP stations: Ada, Adana; Ank, Ankara; Ant, Antalya; Erd, Erdemli; Güz, Güzeloluk; Koç, Koçbeyli; Sin, Sinop. See figure 1 for GNIP station locations, and table 1 for GNIP instrumental records.

Waters sampled between the windward mountain flanks and the evaporation-dominated plateau interior delineate rain shadow areas that can be described by:

$$\text{Leeward Pontic Mountains LMWL: } \delta D = 5.7 \cdot \delta^{18}O - 11.7 \quad (4)$$

$$\text{Leeward Taurus Mountains LMWL: } \delta D = 5.9 \cdot \delta^{18}O - 14.0. \quad (5)$$

Both regions hence represent slightly more arid environmental conditions as compared to the windward mountain flanks and document that secondary evaporation influences the stable isotopic composition of surface water flows sampled on the lee side of both mountain ranges. This influence is reflected in the lower slopes of these two LMWLs when compared to the windward side of the mountain ranges (eqs 1 and 2). Evaporation on the leeward sides however plays a minor role relative to the central plateau region. This is manifested by the different slopes of the LWMLs in the plateau interior and the leeward sides (4.0 versus 5.7 and 5.9; eqs 3 to 5).

A comparison of the geographical extent of the zones, based on the classification above (fig. 6), shows that while in the north both the windward and the leeward zones are largely parallel to the Pontic Mountain range, in the south only the windward zone runs parallel to the Taurus Mountain range. The leeward zone, based on its LMWL, is developed only in the eastern part of the CAP, immediately leeward of the Taurus Mountain range, whereas in the western part, the Plateau Interior Zone connects

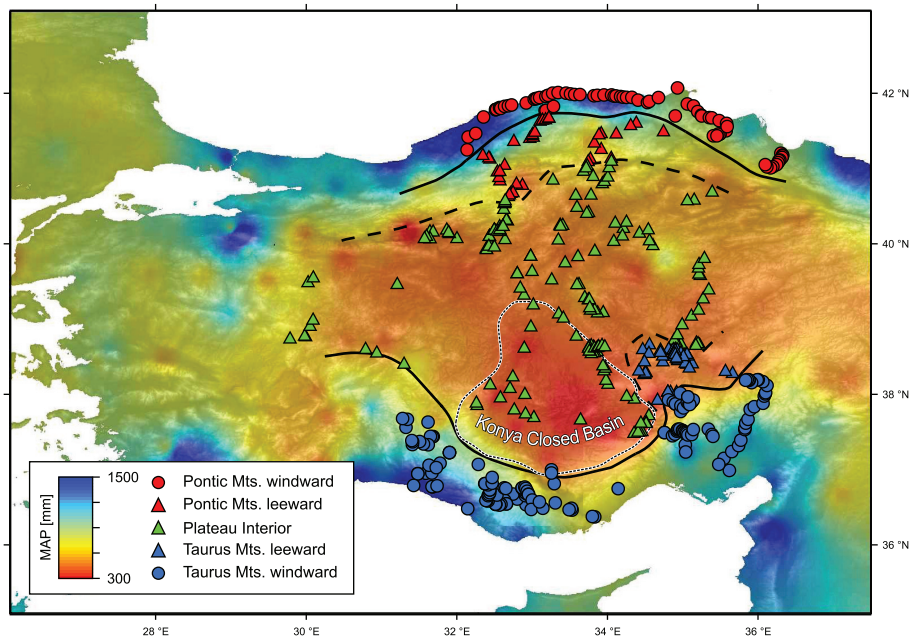

Fig. 6. Meteoric water isotopic regimes over Central Anatolia as derived from the analysis of the Meteoric Water Lines, and compared to the distribution of the mean annual precipitation (MAP).

directly to the Taurus Mountains. δD and $\delta^{18}O$ values in this area, corresponding to the Konya Closed Basin, define a LMWL of $\delta D = 4.1 \cdot \delta^{18}O - 28.0$, which is in very good agreement with the Plateau Interior LMWL (eq 3). This reflects an evaporative climatic regime for the Konya Closed Basin comparable to the Plateau interior, well in line with its very low MAT and MAP values.

Constraining Isotopic Lapse Rates Using Average Catchment Elevations

A cornerstone in paleoaltimetry is a robust characterization of the altitude effect on hydrogen and oxygen isotopes in precipitation ("isotopic lapse rate"). Previous studies applied various methods to constrain the isotopic lapse rate of orographic precipitation, using thermodynamic approaches (Rowley and Garzione, 2007 with references therein) or empirical estimations based on stable isotopic data of precipitation and surface runoff (for example, Poage and Chamberlain, 2001; Quade and others, 2007; Hren and others, 2009; Quade and others, 2011). Since stable isotope paleoaltimetry ultimately yields precipitation-weighted hypsometric mean elevations, reflecting the interplay of topography, relief, and rainfall patterns in mountain ranges, we calculate upstream catchment elevations for each sampling point along individual drainages (see METHODS section). Calculated average catchment elevations (ACEs) for all 180 surface water samples exceed the sampling elevations by about 510 m on average. The ACEs for the 302 spring waters however are, on average, only 23 m above the corresponding sampling elevations. This is mainly due to the fact that (1) the GIS-based hydrological approach applied here only takes geomorphology into account and that (2) no detailed constraints exist for groundwater flow paths and subsurface hydraulics within the small catchments. Since the δD and $\delta^{18}O$ values of springs are usually lower than those of the nearby surface water flows, the springs likely represent precipitation recharged at elevations higher than suggested by the calculated ACEs

(fig. 7). Therefore, the actual catchment areas of the sampled springs should be considerably larger than calculated and, especially in the high-relief areas of the Taurus and Pontic Mountains, their average catchment elevations are also most likely higher than predicted by our model.

In table 2, we compare linear correlation coefficients between isotopic compositions and the two different types of elevation information. As expected, the correlation between elevation and isotopic composition of meteoric water significantly increases for streams and creeks if ACEs rather than actual sampling elevations are taken, whereas no improvement is evident for springs. In order to account for the difficulties inherent to integrating spring samples with catchment elevation information, all relevant calculations are based here on ACEs for surface water samples only.

Figure 7 shows the relationship of catchment elevation with isotopic fractionation of hydrogen and oxygen in modern meteoric waters of the Taurus and Pontic Mountains, for an elevation range from sea-level up to approximately 2700 m (Taurus Mountains) and 1400 m (Pontic Mountains). Based on the paucity of samples from surface water flows in the Pontic Mountains we focused on two transects for the lapse rate calculation (western and eastern transect in fig. 6C; table A2 in the electronic supplementary material; http://earth.geology.yale.edu/~ajs/SupplementaryData/2013/01Schemmel.pdf). Isotopic lapse rates of about −20‰/km for δD and −2.9‰/km for $\delta^{18}O$ in the Taurus Mountains, as well as −19‰/km for δD and −2.6‰/km for $\delta^{18}O$ in the Pontic Mountains are in good agreement with the global average on the windward side of major mountain belts of −2.8‰/km for $\delta^{18}O$ (Poage and Chamberlain, 2001; Lechler and Niemi, 2011). The near-sea level δD and $\delta^{18}O$ values of the Taurus and Pontic precipitation trends are based on the robust, long-term (multi-year to decadal) precipitation record of the GNIP stations at the Black Sea (Sinop) and Mediterranean Sea coasts (Adana) (table 1). Forcing a linear regression through these near-sea level values, the elevation-dependent hydrogen and oxygen isotope fractionation is reasonably close to that derived from thermodynamic considerations (Rowley and others, 2001; Currie and others, 2005; Rowley and Garzione 2007) as well as that from empirical datasets in major mountain ranges (Poage and Chamberlain, 2001).

challenges and perspectives for stable isotope paleoaltimetry

The present-day topography of the CAP is well reflected in the spatial patterns of δD and $\delta^{18}O$ of meteoric waters. Samples collected from the windward flanks of both mountain ranges show the distinct isotopic fingerprint of different air masses and upstream moisture trajectories. First, stable isotope lapse rates calculated from surface runoff are consistent with the present-day global average in larger mountain belts. Second, the spatial distribution of water samples analyzed in this study outlines two regions of isotopic rain shadows in the lee of either mountain range that provide reliable first-order information on upstream depletion in D and ^{18}O due to orographic rainfall (leeward flanks in fig. 6). Both, windward slope isotope-elevation relationships (for example, Mulch and others, 2006) and temporally transient leeward depletion patterns in D and ^{18}O ("isotopic rain shadow"; for example, Chamberlain and others, 1999; Poage and Chamberlain, 2002) currently record the impact of present-day topography. Assuming that no major changes in large-scale Northern hemisphere atmospheric circulation patterns have occurred over the (Late) Neogene (at least on tectonic timescales and rates; Micheels and others, 2011) stable isotope paleoaltimetry approaches have a high potential of detecting changing rainout and aridity patterns along the plateau margins and within the rain shadow regions of the plateau interior through time. Under the current climate and hydrologic conditions, however, the strong evaporative enrichment in ^{18}O (and to a lesser degree D) in surface water flows of the central part of the CAP would render stable isotope paleoaltimetry approaches

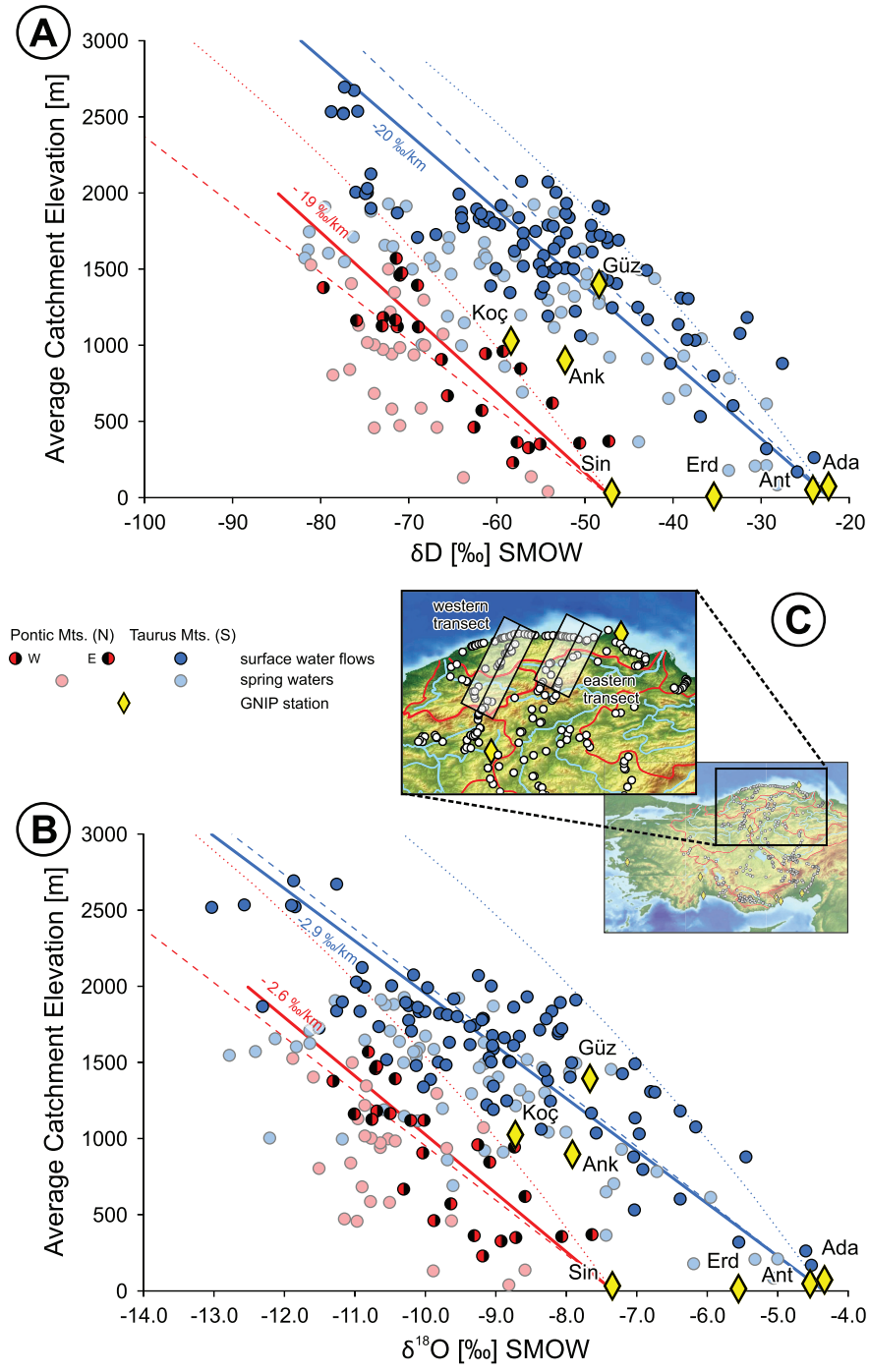

Fig. 7. (A) δD and (B) $\delta^{18}O$ versus average catchment elevation of water samples collected on the northern (two individual transects plotted together, $n_{springs} = 26$, $n_{surface\ water\ flows} = 26$) and southern plateau margins ($n_{springs} = 61$, $n_{surface\ water\ flows} = 93$). Isotopic lapse rates are based on surface water flows only indicated by solid lines and are compared to the precipitation trends by Poage and Chamberlain (2001) (dashed lines) as well as Currie and others (2005) (dotted lines). The initial—sea-level—isotopic compositions correspond to long-term average precipitation records from the coastal GNIP stations Sinop (Pontic Mts.) and Adana (Taurus Mts.) (IAEA/WMO, 2006). Abbreviations of the GNIP stations as in figure 5; see figure 1 for GNIP station locations, and table 1 for GNIP instrumental records.

TABLE 2

Linear correlation coefficients (R^2) between isotopic composition and sampling elevation (SE) as well as average catchment elevation (ACE) for all samples from the windward flanks of the Pontic and Taurus Mountains

	n		R^2 of δD values				R^2 of $\delta^{18}O$ values			
	springs	surface waters	springs		surface water flows		springs		surface water flows	
			SE	ACE	SE	ACE	SE	ACE	SE	ACE
Pontic Mts., windward	33	40	0.51	0.50	0.03	0.32	0.48	0.47	0.02	0.20
Taurus Mts., windward	61	93	0.58	0.56	0.41	0.74	0.51	0.51	0.36	0.68

challenging at best. In addition, the strong evaporative influence on the stable isotopic composition of meteoric waters makes the CAP comparable to other major plateaus on Earth; for example, the Tibetan Plateau (Quade and others, 2011). Both share general topographic (bordered by orographic barriers, relatively uniform plateau elevations) and certain climatological similarities (steep negative precipitation gradient towards the arid plateau interiors, evaporative effect on meteoric water δD and $\delta^{18}O$ values). At present, however, mixing between southeasterly derived summer monsoon air masses and springtime precipitation from westerly marine or continental sources explains some of the observed variation in Tibet (Quade and others, 2011) whereas the influence of air mass mixing on isotopic patterns on the CAP does not appear to play a dominant role. To some degree these differences in meteoric water isotopic patterns on the CAP and Tibet are most likely caused by the difference in the prevailing temperatures and hence, the precipitation-evaporation balance between the two plateau regions, ultimately controlled by plateau elevation. The Tibetan Plateau stands at about 4500 m whereas the CAP reaches only about 1000 m average elevation, leading to a MAT below 0 °C for the most part of the Tibetan Plateau and to about 9 to 12 °C for the CAP along with a clearly higher difference between MAT and mean summer temperatures. We suggest that the CAP is a prominent example of an initial stage of plateau growth where (semi) arid conditions prevail that are accompanied by evaporation as the main process shaping the stable isotopic composition of meteoric waters. During later stages of plateau uplift, temperature decrease restricts the influence of evaporative processes on isotopic fractionation, allowing air mass mixing to become increasingly dominant for meteoric δD and $\delta^{18}O$ patterns.

Despite the relatively simple first-order rainfall–topography relationships characteristic for the CAP, in the following we would like to highlight two further observations that have more general implications for stable isotope paleoaltimetry in orogenic plateau regions.

The Role of Winter Recharge for δD and $\delta^{18}O$ of Near-Surface Groundwater

Spring and surface water samples from the central CAP (Ankara) region display a bias towards mean monthly winter precipitation δD and $\delta^{18}O$ values when compared to the rainfall data from the Ankara GNIP station (fig. 8). We interpret this bias to result from the strongly seasonal (winter dominant) rainfall pattern along the CAP margins and within the CAP interior that ultimately results in a positive precipitation-evaporation balance during the cold season and winter-dominated groundwater

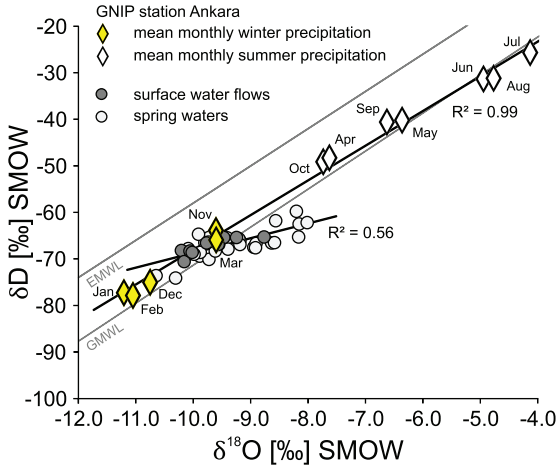

Fig. 8. δD versus $\delta^{18}O$ of water samples collected in a 70 km radius around the GNIP station in Ankara (IAEA/WMO, 2006) compared to the mean monthly precipitation recorded at this station. Note that the sample data form an array that best corresponds to the mean winter (December to May) precipitation values.

recharge. A seasonal bias in both rainfall (as well as groundwater recharge) and mineral proxy formation has implications for oxygen and hydrogen isotope paleoclimate and paleoelevation records. First, winter dominance of low-δD and low-$\delta^{18}O$ groundwater recharge dampens any potential signal of evaporative conditions in the plateau interior and may mask the onset of continental aridity as typically seen in high-elevation plateau regions. For our present-day CAP stable isotope record, winter-dominated groundwater recharge (and associated runoff) implies that the observed convex isotope versus distance pattern (between about 300 to 600 km in figs. 3C and 3D) actually underestimates the amount of evaporative enrichment in D and ^{18}O within the plateau interior. If similar seasonality prevailed during the geologic past, such conditions would bias individual stable isotope paleoaltimetry proxies in different ways: proxies from lacustrine or alluvial environments would record the combined effects of (distal) winter-dominated runoff (negative bias in $\delta^{18}O$) and lake water evaporation (positive bias in $\delta^{18}O$) whereas pedogenic or authigenic minerals that grow in soils actually record local soil water conditions during the time of mineral growth. Pedogenic carbonates as an example are a common stable isotope paleoaltimetry proxy, yet with a strongly seasonal (warm season-dominated) growth pattern (Breecker and others, 2009). We would like to point out that any stable isotope paleoaltimetry reconstruction based solely on records within plateau interiors will be affected by such seasonality effects. For the CAP we conclude that analysis of $\delta^{18}O$ (and to a lesser degree δD) values of pedogenic proxy minerals within the plateau interior requires consideration of rainfall seasonality including a variably strong bias towards winter precipitation even during warm season growth of the proxy minerals.

Topographically Driven Subsurface Groundwater Flow

Topographically driven subsurface groundwater flow characterizes the near surface hydrology in the catchment that feeds the fault-controlled Konya and Tuz Gölü basins (figs. 4 and 6; Bayari and others, 2009). Radiocarbon and stable isotope data for modern groundwater indicate that subsurface flow induces "transported" hydrogen and oxygen isotopic signals that blur the real extent of the isotopic rain shadow (figs. 3 and 4). The large hydraulic head between the recharge (Taurus Mountains) and

discharge (Konya Closed Basin) areas induces a pattern of northward increasing radiocarbon groundwater ages and decreasing $\delta^{18}O$ values with increasing distance from the high-elevation Taurus range (Bayari and others, 2009). Interestingly, springs near Tuz Gölü that are fed by the deepest aquifers (1) originating at high elevations in the Taurus Mountains and (2) characterized by the oldest radiocarbon ages (and hence the longest subsurface residence and travel times) show *d* values characteristic for the leeward rain shadow region of the Taurus Mountains and hence a Mediterranean moisture source (Bayari and others, 2009; best seen between about 150 and 400 km in figs. 3C, 3D, and 4). We consider it very likely that this subsurface flow pattern has been in place at least since adequate topographic gradients have existed between the southern CAP margin (Taurus Mountains) and the CAP interior (Tuz Gölü) which date back up to about 8 Ma; when deposition of marine sediments onlapping the Taurus basement ceased and surface uplift of the Central Taurus Mountains most likely commenced (Cosentino and others, 2012). Therefore, fault-bounded mineralizations (for example, calcite cements, secondary groundwater precipitates and their fluid inclusions) in low-elevation discharge areas of fault-controlled groundwater flow (for example, along the NW-trending Tuz Gölü Fault at the E margin of the Tuz Gölü Basin) may be potential candidates for paleoclimate (paleo-groundwater composition) and stable isotope paleoaltimetry applications. This may be a general feature of plateau margins where relatively simple topographic and hydraulic gradients characterize range-to-basin groundwater flow in continental plateau interiors and provides additional opportunity for stable isotope paleoclimate/paleoaltimetry reconstructions in places where secondary evaporation of, for example, lake and soil waters renders stable isotope proxy results in lacustrine or pedogenic environments questionable.

CONCLUSIONS

We present the first comprehensive hydrogen (δD) and oxygen ($\delta^{18}O$) isotope dataset of modern meteoric waters (streams, creeks, and springs in small catchments) from the Central Anatolian Plateau (CAP) and its orographically accentuated margins with special emphasis on rainfall-topography relationships along the CAP margins. Hydrogen and oxygen isotope analysis of more than 480 stream, creek, and spring water samples allows us to establish a first-order isotopic template for the plateau region which may serve as a reference against which paleoelevation proxy data recovered from, for example, paleosols, fossil teeth, and lipids may be more accurately interpreted and tested. The ability of our data to reliably mirror longer-term, catchment-specific isotopic patterns on an annual to decadal scale, unbiased by sub-annual hydrometeorologically-driven fluctuations, is warranted by a comparison to long-term rainfall data series recorded at the stations of the Global Network of Isotopes in Precipitation (GNIP).

Central Anatolia exhibits a characteristic pattern of orographic rainout, isotopic rain shadow development as well as secondary evaporation, strongly controlled by its modern topographic and climatic setting. We identify "quasi-symmetrical" isotopic lapse rates at the S and N margins of the CAP with $-20‰$/km (δD) and $-2.9‰$/km ($\delta^{18}O$), as well as $-19‰$/km (δD) and $-2.6‰$/km ($\delta^{18}O$), respectively. However, moisture entering the plateau from the S is isotopically distinct from that derived from sources to the N with $\Delta(\delta D_{N-S})$ of about 20 permil and $\Delta(\delta^{18}O_{N-S})$ of about 3 permil when measured at sea level. The semi-arid plateau interior with a mean precipitation rate as low as 300 to 500 mm/yr and mean summer temperatures attaining 23 °C, undergoes severe sub-cloud and/or surface evaporation as evidenced by systematic enrichment in D and ^{18}O in surface runoff.

The regional δD and $\delta^{18}O$ patterns of present-day meteoric water as a result of up-slope distillation during orographic rainout and individual low-elevation starting compositions dependent on moisture source and upstream air parcel trajectories can

be a powerful tool for reconstructing paleoaltimetry of the CAP despite its moderate size and geographic location relative to dominant air-parcel trajectories. The preservation potential of any paleoprecipitation proxy material on the uplifting margins of the CAP seems moderate, but the windward sides of the plateau margins and the "isotopic rain shadows" on their leeward sides are both prime candidates to retain non-evaporative isotopic signals of past precipitation.

ACKNOWLEDGMENTS

AM acknowledges support through DFG-MU 2845/1-1 and the European Science Foundation Topo Europe initiative. This study was supported through the LOEWE funding program of Hesse's Ministry of Higher Education, Research, and the Arts. The ASTER GDEM data used in this study are a property of the Ministry of Economy, Trade, and Industry of Japan (METI) and NASA. Details on the implementation of the ACE calculation provided by T. Schildgen (Potsdam) were invaluable. M. Demircan (State Meteorological Service, Ankara) generously provided long-term temperature and precipitation data of Turkey. T. Chavez and S. Terzer (IAEA, Vienna) kindly provided us with the latest GNIP datasets. Thanks are extended to C. Wenske (Hannover) and U. Treffert (Frankfurt) for laboratory support. The paper benefited from thoughtful field discussions with the Topo Europe Vertical Anatolian Movements Project members, as well as from the detailed, very constructive reviews of D. Breecker, and A. Lechler.

References

Bayari, C. S., Ozyurt, N. N., and Kilani, S., 2009, Radiocarbon age distribution of groundwater in the Konya Closed Basin, central Anatolia, Turkey: Hydrogeology Journal, v. 17, n. 2, p. 347–365, http://dx.doi.org/10.1007/s10040-008-0358-2

Biryol, C. B., Beck, S. L., Zandt, G., and Özacar, A. A., 2011, Segmented African lithosphere beneath the Anatolian region inferred from teleseismic P-wave tomography: Geophysical Journal International, v. 184, n. 3, p. 1037–1057, http://dx.doi.org/10.1111/j.1365-246X.2010.04910.x

Blisniuk, P. M., and Stern, L. A., 2005, Stable isotope paleoaltimetry: A critical review: American Journal of Science, v. 305, n. 10, p. 1033–1074, http://dx.doi.org/10.2475/ajs.305.10.1033

Breecker, D. O., Sharp, Z. D., and McFadden, L. D., 2009, Seasonal bias in the formation and stable isotopic composition of pedogenic carbonate in modern soils from central New Mexico, USA: Geological Society of America Bulletin, v. 121, n. 3–4, p. 630–640, http://dx.doi.org/10.1130/B26413.1

Campani, M., Mulch, A., Kempf, O., Schlunegger, F., and Mancktelow, N., 2012, Miocene paleotopography of the Central Alps: Earth and Planetary Science Letters, v. 337–338, p. 174–185, http://dx.doi.org/10.1016/j.epsl.2012.05.017

Cavazza, W., Federici, I., Okay, A. I., and Zattin, M., 2011, Apatite fission-track thermochronology of the Western Pontides (NW Turkey): Geological Magazine, v. 149, n. 1, p. 133–140, http://dx.doi.org/10.1017/S0016756811000525

Chamberlain, C. P., Poage, M. A., Craw, D., and Reynolds, R. C., 1999, Topographic development of the Southern Alps recorded by the isotopic composition of authigenic clay minerals, South Island, New Zealand: Chemical Geology, v. 155, n. 3–4, p. 297–294, http://dx.doi.org/10.1016/S0009-2541(98)00165-X

Cosentino, D., Schildgen, T. F., Cipollari, P., Faranda, C., Gliozzi, E., Hudáčková, N., Lucifora, S., and Strecker, M. R., 2012, Late Miocene surface uplift of the southern margin of the Central Anatolian Plateau, Central Taurides, Turkey: Geological Society of America Bulletin, v. 124, n. 1–2, p. 133–145, http://dx.doi.org/10.1130/B30466.1

Craig, H., 1961, Isotopic variations in meteoric waters: Science, v. 133, n. 3465, p. 1702–1703, http://dx.doi.org/10.1126/science.133.3465.1702

Craig, H., and Gordon, L. I., 1965, Deuterium and oxygen-18 variations in the ocean and the marine atmosphere, *in* Tongiorgi, E., editor, Stable Isotopes in Oceanographic Studies and Paleotemperatures: Pisa, Consiglio Nazionale delle Riche, Laboratorio de Geologia Nucleare, p. 1–122.

Currie, B. S., Rowley, D. B., and Tabor, N. J., 2005, Middle Miocene paleoaltimetry of southern Tibet: Implications for the role of mantle thickening and delamination in the Himalayan orogen: Geology, v. 33, n. 3, p. 181–184, http://dx.doi.org/10.1130/G21170.1

Cyr, A. J., Currie, B. S., and Rowley, D. B., 2005, Geochemical evaluation of Fenghuoshan Group lacustrine carbonates, north-central Tibet: Implications for the paleoaltimetry of Late Eocene Tibetan Plateau: Journal of Geology, v. 113, n. 5, p. 517–533, http://dx.doi.org/10.1086/431907

Dansgaard, W., 1964, Stable isotopes in precipitation: Tellus, v. 16, n. 4, p. 436–468, http://dx.doi.org/10.1111/j.2153-3490.1964.tb00181.x

Dirican, A., Ünal, S., Acar, Y., and Demircan, M., 2005, The temporal and seasonal variation of H-2 and O-18

in atmospheric water vapour and precipitation from Ankara, Turkey in relation to air mass trajectories at Mediterranean Basin, *in* IAEA-TECDOC-1453, Isotopic Composition of Precipitation in the Mediterranean Basin in Relation to Air Circulation Patterns and Climate: Vienna, International Atomic Energy Agency, p. 191–215, available online at: www-pub.iaea.org/MTCD/publications/PDF/te_1453_web.pdf

Ehlers, T. A., and Poulsen, C. J., 2009, Influence of Andean uplift on climate and paleoaltimetry estimates: Earth and Planetary Science Letters, v. 281, n. 3–4, p. 238–248, http://dx.doi.org/10.1016/j.epsl.2009.02.026

Galewsky, J., 2009, Orographic precipitation isotopic ratios in stratified atmospheric flows: Implications for paleoelevation studies: Geology, v. 37, n. 9, p. 791–794, http://dx.doi.org/10.1130/G30008A.1

Gans, C. R., Beck, S. L., Zandt, G., Biryol, C. B., and Özacar, A. A., 2009, Detecting the limit of slab break-off in central Turkey: New high-resolution *Pn* tomography results: Geophysical Journal International, v. 179, n. 3, p. 1566–1572, http://dx.doi.org/10.1111/j.1365-246X.2009.04389.x

Garzione, C. N., Dettman, D. L., Quade, J., DeCelles, P. G., and Butler, R. F., 2000a, High times on the Tibetan Plateau: Paleoelevation of the Thakkhola graben, Nepal: Geology, v. 28, n. 4, p. 339–342, http://dx.doi.org/10.1130/0091-7613(2000)28⟨339:HTOTTP⟩2.0.CO;2

Garzione, C. N., Quade, J., DeCelles, P. G., and English, N. B., 2000b, Predicting paleoelevation of Tibet and the Himalaya from $\delta^{18}O$ vs. altitude gradients in meteoric water across the Nepal Himalaya: Earth and Planetary Science Letters, v. 183, n. 1–2, p. 215–229, http://dx.doi.org/10.1016/S0012-821X(00)00252-1

Garzione C. N., Molnar, P., Libarkin, J. C., and MacFadden, B. J., 2006, Rapid late Miocene rise of the Bolivian Altiplano: Evidence for removal of mantle lithosphere: Earth and Planetary Science Letters, v. 241, n. 3–4, p. 543–556, http://dx.doi.org/10.1016/j.epsl.2005.11.026

Garzione, C. N., Hoke, G. D., Libarkin, J. C., Withers, S., MacFadden, B. J., Eiler, J., Ghosh, P., and Mulch, A., 2008, Rise of the Andes: Science, v. 320, n. 5881, p. 1304–1307, http://dx.doi.org/10.1126/science.1148615

Gat, J., and Carmi, I., 1970, Evolution of the isotopic composition of atmospheric waters in the Mediterranean Sea area: Journal of Geophysical Research, v. 75, n. 15, p. 3039–3048, http://dx.doi.org/10.1029/JC075i015p03039

Gat, J. R., Klein, B., Kushnir, Y., Roether, W., Wernli, H., Yam, R., and Shemesh, A., 2003, Isotope composition of air moisture over the Mediterranean Sea: An index of the air-sea interaction pattern: Tellus, v. 55B, p. 953–965, http://dx.doi.org/10.1034/j.1600-0889.2003.00081.x

Görür, N., and Tüysüz, O., 2001, Cretaceous to Miocene palaeogeographic evolution of Turkey: implications for hydrocarbon potential: Journal of Petroleum Geology, v. 24, n. 2, p. 119–146, http://dx.doi.org/10.1111/j.1747-5457.2001.tb00664.x

Görür, N., Sakınç, M., Barka, A., Akkök, R., and Ersoy, Ş., 1995, Miocene to Pliocene palaeogeographic evolution of Turkey and its surroundings: Journal of Human Evolution, v. 28, n. 4, p. 309–324, http://dx.doi.org/10.1006/jhev.1995.1025

Horton, T. W., Sjostrom, D. J., Abruzzese, M. J., Poage, M. A., Waldbauer, J. R., Hren, M., Wooden, J., and Chamberlain, C. P., 2004, Spatial and temporal variation of Cenozoic surface elevation in the Great Basin and Sierra Nevada: American Journal of Science, v. 304, n. 10, p. 862–888, http://dx.doi.org/10.2475/ajs.304.10.862

Hren, M. T., Bookhagen, B., Blisniuk, P. M., Booth, A. L., and Chamberlain, C. P., 2009, $\delta^{18}O$ and δD of streamwaters across the Himalaya and Tibetan Plateau: Implications for moisture sources and paleoelevation reconstructions: Earth and Planetary Science Letters, v. 288, n. 1–2, p. 20–32, http://dx.doi.org/10.1016/j.epsl.2009.08.041

IAEA/WMO, 2006, Global Network of Isotopes in Precipitation—The GNIP Database, available online at: http://www.iaea.org/water

Ingraham, N. L., and Taylor, B. E., 1991, Light stable isotope systematics of large-scale hydrologic regimes in California and Nevada: Water Resources Research, v. 27, n. 1, p. 77–90, http://dx.doi.org/10.1029/90WR01708

Insel, N., Poulsen, C., and Ehlers, T., 2009, Influence of the Andes Mountains on South American moisture transport, convection, and precipitation: Climate Dynamics, v. 35, n. 7–8, p. 1477–1492, http://dx.doi.org/10.1007/s00382-009-0637-1

Kendall, C., and Coplen, T. B., 2001, Distribution of oxygen-18 and deuterium in river waters across the United States: Hydrological Processes, v. 15, n. 7, p. 1363–1393, http://dx.doi.org/10.1002/hyp.217

Lechler, A. R., and Niemi, N. A., 2011, Controls on the spatial variability of modern meteoric $\delta^{18}O$: Empirical constraints from the western U.S. and East Asia and implications for stable isotope studies: American Journal of Science, v. 311, n. 8, p. 664–700, http://dx.doi.org/10.2475/08.2011.02

Lüttig, G., and Steffens, P., 1975, Paleogeographic Atlas of Turkey from the Oligocene to the Pleistocene: Hannover, Germany, Bundesanstalt für Geowissenschaften und Rohstoffe, 64 p.

Micheels, A., Bruch, A. A., Eronen, J., Fortelius, M., Harzhauser, M., Utescher, T., and Mosbrugger, V., 2011, Analysis of heat transport mechanisms from a Late Miocene model experiment with a fully-coupled atmosphere-ocean general circulation model: Palaeogeography, Palaeoclimatology, Palaeoecology, v. 304, n. 3–4, p. 337–350, http://dx.doi.org/10.1016/j.palaeo.2010.09.021

Mix, H. T., Mulch, A., Kent-Corson, M. L., and Chamberlain, C. P., 2011, Cenozoic migration of topography in the North American Cordillera: Geology, v. 39, n. 1, p. 87–90, http://dx.doi.org/10.1130/G31450.1

Mulch, A., and Chamberlain, C. P., 2007, Stable isotope paleoaltimetry in orogenic belts—The silicate record in surface and crustal geological archives: Reviews in Mineralogy and Geochemistry, v. 66, n. 1, p. 89–118, http://dx.doi.org/10.2138/rmg.2007.66.4

Mulch, A., Graham, S. A., and Chamberlain, C. P., 2006, Hydrogen isotopes in Eocene river gravels and paleoelevation of the Sierra Nevada: Science, v. 313, n. 5783, p. 87–89, http://dx.doi.org/10.1126/science.1125986

Mulch, A., Sarna-Wojcicki, A. M., Perkins, M. E., and Chamberlain, C. P., 2008, A Miocene to Pleistocene

climate and elevation record of the Sierra Nevada (California): Proceedings of the National Academy of Sciences of the United States of America, v. 105, n. 19, p. 6819–6824, http://dx.doi.org/10.1073/pnas.0708811105
Mulch, A., Uba, C. E, Strecker, M. R., Schoenberg, R., and Chamberlain, C. P., 2010, Late Miocene climate variability and surface elevation in the central Andes: Earth and Planetary Science Letters, v. 290, n. 1–2, p. 173–182, http://dx.doi.org/10.1016/j.epsl.2009.12.019
Müller, U. C., Pross, J., Tzedakis, P. C., Gamble, C., Kotthoff, U., Schmiedl, G., Wulf, S., and Christanis, K., 2011, The role of climate in the spread of modern humans into Europe: Quarternary Science Reviews, v. 30, n. 3–4, p. 273–279, http://dx.doi.org/10.1016/j.quascirev.2010.11.016
Pfahl, S., and Wernli, H., 2008, Air parcel trajectory analysis of stable isotopes in water vapor in the Eastern Mediterranean: Journal of Geophysical Research: Atmospheres, v. 113, n. D20, p. 1–6, http://dx.doi.org/10.1029/2008JD009839
Poage, M. A., and Chamberlain, C. P., 2001, Empirical relationships between elevation and the stable isotope composition of precipitation and surface waters: Considerations for studies of paleoelevation change: American Journal of Science, v. 301, n. 1, p. 1–15, http://dx.doi.org/10.2475/ajs.301.1.1
——— 2002, Stable isotopic evidence for a pre-Middle Miocene rain shadow in the western Basin and Range: Implications for the paleotopography of the Sierra Nevada: Tectonics, v. 21, n. 4, p. 1–10, http://dx.doi.org/10.1029/2001TC001303
Poulsen, C. J., Ehlers, T. A., and Insel, N., 2010, Onset of convective rainfall during gradual late Miocene rise of the central Andes: Science, v. 328, n. 5977, p. 490–493, http://dx.doi.org/10.1126/science.1185078
Quade, J., Garzione, C., and Eiler, J., 2007, Paleoelevation reconstruction using pedogenic carbonates: Reviews in Mineralogy and Geochemistry, v. 66, n. 1, p. 53–87, http://dx.doi.org/10.2138/rmg.2007.66.3
Quade, J., Breecker, D. O., Daeron, M., and Eiler, J., 2011, The paleoaltimetry of Tibet: An isotopic perspective: American Journal of Science, v. 311, n. 2, p. 77–115, http://dx.doi.org/10.2475/02.2011.01
Rindsberger, M., Magaritz, M., Carmi, I., and Gilad, D., 1983, The relation between air mass trajectories and the water isotope composition of rain in the Mediterranean Sea area: Geophysical Research Letters, v. 10, n. 1, p. 43–46, http://dx.doi.org/10.1029/GL010i001p00043
Rowley, D. B., and Currie, B. S., 2006, Paleo-altimetry of the late Eocene to Miocene Lunpola Basin, central Tibet: Nature, v. 439, p. 677–681, http://dx.doi.org/10.1038/nature04506
Rowley, D. B., and Garzione, C. N., 2007, Stable isotope-based paleoaltimetry: Annual Review of Earth and Planetary Sciences, v. 35, p. 463–508, http://dx.doi.org/10.1146/annurev.earth.35.031306.140155
Rowley, D. B., Pierrehumbert, R. T., and Currie, B. S., 2001, A new approach to stable isotope based paleoaltimetry: implications for paleoaltimetry and paleohypsometry of the High Himalaya since the Late Miocene: Earth and Planetary Science Letters, v. 188, n. 1–2, p. 253–268, http://dx.doi.org/10.1016/S0012-821X(01)00324-7
Rozanski, K., Araguás-Araguás, L., and Gonfiantini, R., 1993, Isotopic patterns in modern global precipitation, *in* Swart, P. K., Lohmann, K. C., McKenzie, J., and Savin, S., editors, Climate Change in Continental Isotopic Records: Geophysical Monograph Series, v. 78, p. 1–36, http://dx.doi.org/10.1029/GM078p0001
Sariş, F., Hannah, D. M., and Eastwood, W. J., 2010, Spatial variability of precipitation regimes over Turkey: Hydrological Sciences Journal, v. 55, n. 2, p. 234–249 http://dx.doi.org/10.1080/02626660903546142
Schildgen, T. F., Cosentino, D., Bookhagen, B., Niedermann, S., Yildirim, C., Echtler, H., Wittmann, H., and Strecker, M. R., 2012a, Mutli-phased uplift of the southern margin of the Central Anatolian plateau, Turkey: A record of tectonic and upper mantle processes: Earth and Planetary Science Letters, v. 317–318, p. 85–95, http://dx.doi.org/10.1016/j.epsl.2011.12.003
Schildgen, T. F., Cosentino, D., Caruso, A. Buchwaldt, R. Yildirim, C., Bowring, S. A., Rojay, B., Echtler, H., and Strecker, M. R., 2012b, Surface expression of eastern Mediterranean slab dynamics: Neogene topographic and structural evolution of the southwest margin of the Central Anatolian Plateau, Turkey: Tectonics, v. 31, p. 1–21.
Şengör, A. M. C., Tüysüz, O., İmren, C., Sakınç, M., Eyidoğan, H., Görür, N., Le Pichon, X., and Rangin, C., 2005, The North Anatolian fault: A new look: Annual Review of Earth and Planetary Sciences, v. 33, p. 37–112, http://dx.doi.org/10.1146/annurev.earth.32.101802.120415
Sensoy, S., Demircan, M., Ulupinar, Y., and Balta, İ., 2008, Climate of Turkey: Turkish State Meterological Service, Ankara. Retrieved from http://www.dmi.gov.tr/iklim/iklim.aspx on April 24, 2009.
Türkeş, M., 2003, Spatial and temporal variations in precipitation and aridity index series of Turkey *in* Bolle, H.-J., editor, Mediterranean Climate: Variability and Trends. Regional Climate Studies: Heidelberg, Springer, p. 181–213.
Türkeş. M., and Erlat, E., 2005, Climatological responses of winter precipitation in Turkey to variability of the North Atlantic Oscillation during the period 1930–2001: Theoretical and Applied Climatology, v. 81, n. 1–2, p. 45–69, http://dx.doi.org/10.1007/s00704-004-0084-1
Vachon, R. W., Welker, J. M., White, J. W. C., and Vaughn, B. H., 2010, Moisture source temperatures and precipitation $\delta^{18}O$-temperature relationships across the United States: Water Resources Research, v. 46, n. 7, W07523, http://dx.doi.org/10.1029/2009WR008558
Yildirim, C., Schildgen, T. F., Echtler, H., Melnick, D., and Strecker, M. R., 2011, Late Neogene and active orogenic uplift in the Central Pontides associated with the North Anatolian Fault: Implications for the northern margin of the Central Anatolian Plateau, Turkey: Tectonics, v. 30, n. 5, p. TC5005, http://dx.doi.org/10.1029/2010TC002756